Title

Electric-Field-Induced Spatially Dynamic Heterogeneity of Solvent Motion and Cation Transference in Electrolytes

Journal

Physical Review Letters, 128(19)

ISSN

0031-9007

Authors

Halat, David M
Fang, Chao
Hickson, Darby
et al.

Publication Date

2022-05-13

DOI

10.1103/physrevlett.128.198002

Peer reviewed

Electric-Field-Induced Spatially Dynamic Heterogeneity of Solvent Motion and Cation Transference in Electrolytes

David M. Halat,[1,2,*] Chao Fang,[1,2,*] Darby Hickson,[2] Aashutosh Mistry,[3] Jeffrey A. Reimer,[1,2] Nitash P. Balsara,[1,2] and Rui Wang[1,2,†]

[1]*Materials Sciences Division and Joint Center for Energy Storage Research (JCESR), Lawrence Berkeley National Laboratory, Berkeley, California 94720, USA*

[2]*Department of Chemical and Biomolecular Engineering, University of California, Berkeley, Berkeley, California 94720, USA*

[3]*Chemical Sciences and Engineering Division and Joint Center for Energy Storage Research (JCESR), Argonne National Laboratory, Lemont, Illinois 60439, USA*

While electric fields primarily result in migration of charged species in electrolytic solutions, the solutions are dynamically heterogeneous. Solvent molecules within the solvation shells of the cation will be dragged by the field while free solvent molecules will not. We combine electrophoretic NMR measurements of ion and solvent velocities under applied electric fields with molecular dynamics simulations to interrogate different solvation motifs in a model liquid electrolyte. Measured values of the cation transference number (t_+^0) agree quantitatively with simulation-based predictions over a range of electrolyte concentrations. Solvent-cation interactions strongly influence the concentration-dependent behavior of t_+^0. We identify a critical concentration at which most of the solvent molecules lie within solvation shells of the cations. The dynamic heterogeneity of solvent molecules is minimized at this concentration where t_+^0 is approximately equal to zero.

The rate at which secondary batteries can be charged and discharged depends directly on ion transport through the electrolytic phase [1,2]. Ion transport in dilute and concentrated electrolytes is also the subject of intense fundamental interest. In the dilute limit, those solvent molecules within the ion solvation shell will be affected by ion transport, but most will not. In concentrated electrolytes, however, the solvation shells of a fraction of the cations may be composed exclusively of solvent molecules whereas others may contain one or more anions. Thus under application of electric fields, solvent molecules coordinating to cations may be "dragged" with the migrating ion, while those near nominally neutral cation–anion pairs may exhibit weaker coupling to the electric field. The importance of solvent motion was recognized by Hittorf, Onsager, and Newman [3–7]. However, unlike ion motion, which can be readily studied by electrochemical methods, limited direct knowledge exists on solvent motion under applied potential, particularly its heterogeneous nature.

The term "dynamic heterogeneity" is often used to describe spatially heterogeneous dynamics that emerge in glass-forming systems [8,9]. In these systems, dynamics within regions separated by distances of mere nanometers can differ by orders of magnitude. These effects have recently been discovered in other systems such as ionic liquids [10] and solid fast-ion conductors [11]. In the present study, our usage of the term dynamic heterogeneity refers to the fact that the application of an electric field induces motion in some solvent molecules in an electrolyte while others a few nanometers away are unaffected. The disparity in response is related to subtle differences in local environments that surround individual solvent molecules.

In this Letter, we parse solvent motion in the context of ion migration by combining electrophoretic NMR (eNMR) measurements with quiescent molecular dynamics (MD) simulations. To our knowledge, these methods have not yet been applied in a complementary manner to enable a quantitative description of transport of neutral solvent molecules in electrolytes. eNMR enables measurement of the average velocities of the ions and solvent molecules under applied electric fields, whereas the heterogeneity of solvation motifs is quantified by MD simulations. The joint methodology allows determination of the velocity of only those solvent molecules that lie within the cation solvation shell. Comparison of calculated velocities with the averaged species velocities measured by eNMR thus elucidates the dynamic heterogeneity of solvent motion, yielding concentration-dependent structural models that can rationalize electrochemical transport.

A crucial step in our analysis is a comparison of the cation transference numbers determined by experiments and simulations. While conductivity (κ) quantifies ion transport of both the working ion (usually a cation) and the nonworking ion, the parameter that sheds light on the transport of the cation is the transference number (t_+^0), defined as the fraction of ionic current carried by the cation relative to the solvent

velocity in an electrolyte of uniform composition [2]. Recognition of the importance of this transport parameter dates back to Hittorf [3,4]; more recent work has emphasized the relevance of the cation transference number to the electrochemical efficacy of the electrolyte under fast charging conditions [12–14] and circumstances that lead to lithium dendrite growth [15,16]. Newman's concentrated solution theory can be used to relate t_+^0 to species velocities [7,17]. eNMR determines these species velocities when a one-dimensional electric field is applied across an electrolyte of uniform concentration [18–21].

For a binary electrolyte containing a univalent salt of uniform composition,

$$\kappa = \frac{Fc(v_+ - v_-)}{E} \tag{1}$$

and

$$t_+^0 = \frac{v_+ - v_0}{v_+ - v_-}, \tag{2}$$

where v_+, v_-, and v_0 are the averaged species velocities of the cation, anion, and solvent, respectively, F is the Faraday constant, c is salt concentration, and E is the applied electric field [22]. The ionic conductivity and transference number at dilute concentrations can be determined using the Nernst-Einstein equation [23]. For concentrated electrolytes, more rigorous frameworks that capture the ion-ion and the ion-solvent correlations are required [24–29], commonly with the aid of computer simulations [30–34]. In particular, Onsager coefficients, L^{ij}, quantify correlations between species i and j [5,6,35,36]. While several expressions for relating L^{ij} to displacements of species i and j exist, a transparent approach was recently proposed by Fong *et al.* [29,37,38], which expresses L^{ij} as

$$L^{ij} = \frac{Vc_ic_j}{k_BT}\frac{1}{6}\lim_{t\to\infty}\frac{d}{dt}\left\langle \frac{1}{N_i}\sum_\alpha [\boldsymbol{r}_i^\alpha(t) - \boldsymbol{r}_i^\alpha(0)] \cdot \frac{1}{N_j}\sum_\beta [\boldsymbol{r}_j^\beta(t) - \boldsymbol{r}_j^\beta(0)] \right\rangle, \tag{3}$$

where k_B is the Boltzmann constant, T is the temperature, V is the system volume, c_i and N_i are, respectively, the molar concentration and particle number of species i, and $\boldsymbol{r}_i^\alpha(t)$ is the position, relative to the center of mass of the system, for the α^{th} particle of species i at time t. The expression for L^{ij} is analogous to the Nernst-Einstein relation for determining self-diffusion coefficients from mean squared displacements. Experimentally measured conductivity and transference number relative to *solvent* velocity are related to the three independent transport coefficients L^{++}, L^{+-}, and L^{--}, as follows:

$$\kappa = F^2(L^{++} - 2L^{+-} + L^{--}) \tag{4}$$

$$\text{and} \quad t_+^0 = \left(\frac{L^{++} - L^{+-}}{L^{++} - 2L^{+-} + L^{--}} - \omega_-\right)/\omega_0, \tag{5}$$

where ω_- and ω_0 are the mass fractions of anion and solvent, respectively [2,38]. Herein, we explore the consequences of these equations with a joint experimental and computational study of a model electrolyte comprising lithium bis(trifluoromethanesulfonyl)imide (LiTFSI) salt dissolved in tetraglyme (tetraethylene glycol dimethyl ether). We find that we are able to discern the molecular origins of the concentration dependence of t_+^0 in the context of differing molecular structures experienced by the solvent molecules (i.e., dynamic heterogeneity).

Mixtures of LiTFSI and tetraglyme were prepared in a concentration range of 0.18 to 2.5 mol/kg of solvent. In this work, we quantify salt concentration by $r = [\text{Li}^+]/[\text{O}]$, the ratio of Li^+ cations to O atoms within tetraglyme [39–41]. The cation, anion, and solvent may be selectively and unambiguously probed with ^{7}Li, ^{19}F, and ^{1}H NMR measurements, respectively. Our eNMR cell comprises a 5 mm NMR tube with Pt electrodes separated by 3.35 cm [42]. We employ a convection-compensated eNMR pulse sequence [43,44] with bipolar electric field pulses lasting 50 ms for each polarity (Fig. S1 [45]). Temperature, gradient strength, and electric field calibration details are given in the Supplemental Material [45–52]. To minimize systematic errors, measurements were repeated with a range of positive and negative pulsed magnetic field gradient strengths (Figs. S2 and S3 [45]). The eNMR lab-frame velocities thus reflect induced electrophoretic migration during the initial 50 ms of electric field application in an electrolyte of uniform concentration.

Figure 1(a) depicts the average species velocities in LiTFSI/tetraglyme experimentally measured by eNMR. Velocities toward the negative electrode are defined as positive. The anion velocity (v_-) is negative, whereas the cation velocity (v_+) is positive and smaller in magnitude than v_- at all concentrations, consistent with prior literature [53–55]. We also observe an electric field-induced drift of the nominally uncharged solvent. The solvent velocity (v_0) is positive and increases with salt concentration until $r = 0.08$. Thus, the solvent drifts in the same direction as the cation, and moreover, the two velocities become comparable at high salt concentration.

The Onsager transport coefficients L^{++}, L^{+-}, and L^{--} can be determined from MD simulations using the slopes of the term equivalent to mean squared displacement over time, which is defined as

$$\text{MSD}'(t) = \left\langle \begin{matrix} \frac{1}{N_i}\sum_\alpha [\boldsymbol{r}_i^\alpha(t) - \boldsymbol{r}_i^\alpha(0)] \cdot \\ \frac{1}{N_j}\sum_\beta [\boldsymbol{r}_j^\beta(t) - \boldsymbol{r}_j^\beta(0)] \end{matrix} \right\rangle \tag{6}$$

(compare Eq. (3)). Figure 1(b) depicts the MSD′ profiles from MD trajectories at two salt concentrations; Onsager transport

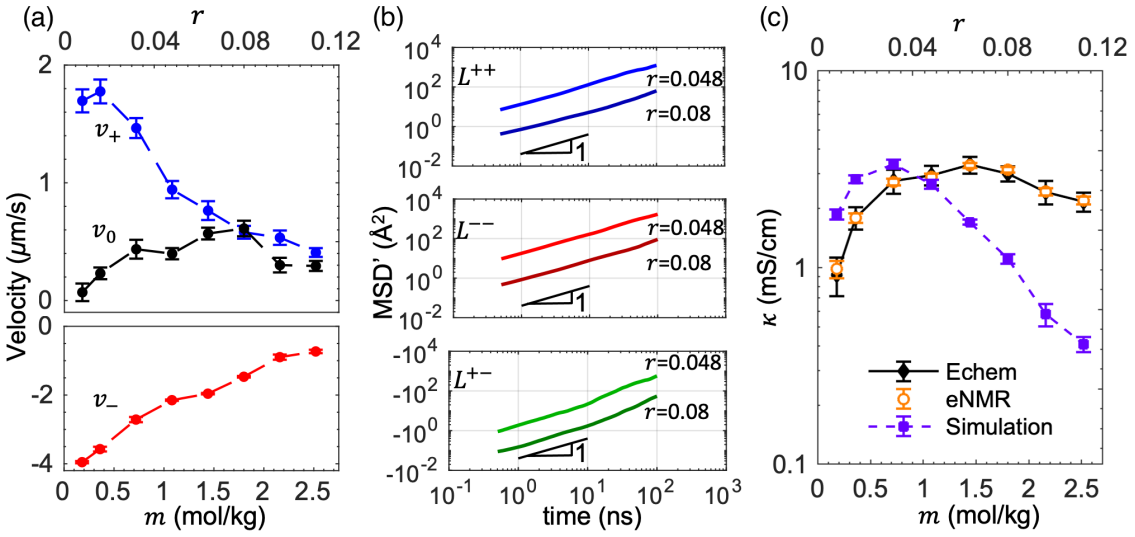

FIG. 1. (a) Average species velocities in LiTFSI/tetraglyme electrolytes ($r = [\mathrm{Li}^+]/[\mathrm{O}]$) measured by ^{7}Li, ^{1}H, and ^{19}F electrophoretic NMR (eNMR) at 30 °C: cation (blue), solvent (black) and anion (red). To highlight the smaller values of v_0 and v_+, a separate vertical axis is plotted for these velocities compared to that for v_-. (See Fig. S4 [45] for data plotted on same axis.) Velocities are in the lab frame of reference. All velocities reflect an applied electric field of 1 V/mm; measurements were performed at a range of electric fields and velocities were scaled to 1 V/mm. (b) Representative MSD′ as defined in Eq. (6) calculated from MD simulations, for $r = 0.048$ (upper traces) and $r = 0.08$ (lower traces), corresponding to Onsager transport coefficients L^{++} (top), L^{--} (middle) and L^{+-} (bottom), which are extracted from the diffusive regime, i.e., the indicated timescale over which the slope equals one in the log-log scale. (c) Ionic conductivity from independent electrochemical and eNMR experiments (filled diamonds and open circles, respectively, which are nearly coincident), and predicted from MD simulations (filled squares).

coefficients are obtained by fitting these curves in the diffusive regime where the MSD′ scales linearly with time. (Further details of the MD simulations are given in the Supplemental Material [45,56–61].) Note that in this approach, solvent mass fraction enters into the expression for t_+^0, and solvent correlations (e.g., L^{+0}) are related to the three independent coefficients, subject to mass balance constraints [38] (see Supplemental Material [45]). The concentration-dependent Onsager transport coefficients are depicted in Fig. S8 [45].

To assess the agreement between the experimental and computational approaches, Fig. 1(c) depicts the ionic conductivity predicted from eNMR velocities and from Onsager transport coefficients [Eqs. (1) and (4)], together with separate electrochemical ac impedance spectroscopy measurements. Agreement between eNMR data and the electrochemical measurements confirms that the eNMR velocities reflect migration of ions; values obtained using these two independent methods are within experimental error at all salt concentrations. The simulation results are in qualitative agreement with experiments, but significant deviations are evident at higher salt concentrations.

Despite the disagreement between conductivity values predicted by experiment and simulation, Fig. 2 reveals remarkable quantitative agreement between t_+^0 obtained from the eNMR species velocities and the Onsager transport coefficients using Eqs. (2) and (5), respectively. The transference number reflects a ratio of transport coefficients, while the conductivity reflects a summation [see Eqs. (4) and (5)]. We arrive at the surprising conclusion that the standard transferable potentials for phase equilibria with united atom (TraPPE-UA) force fields [62–67] are sufficiently accurate to quantitatively capture the underpinnings of an important transport property—the transference number. In Do *et al.* and Brooks *et al.* [68,69], it has been proposed that quantitative agreement between experimentally measured and

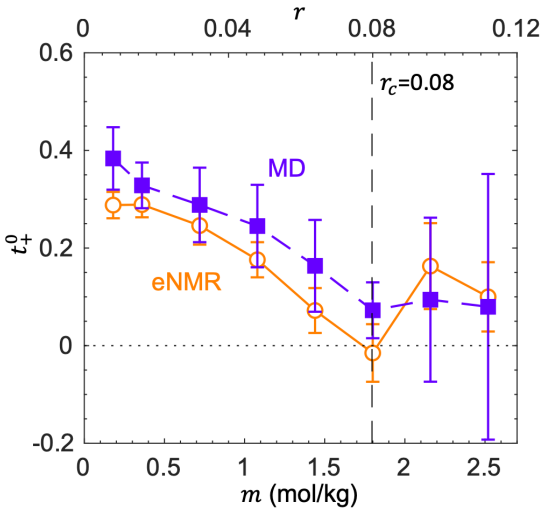

FIG. 2. Transference numbers in the solvent reference frame (t_+^0) determined from eNMR (open symbols) and MD (filled symbols), using Eqs. (2) and (5), respectively. The critical salt concentration, $r_c = 0.08$, is indicated with a dashed line.

simulated conductivities is obtained by rescaling (reducing) the formal charges on the ions. This rescaling is believed to account for the fact that the fixed potentials used to describe interactions in MD simulations do not account for the polarizable nature of atoms and ions. In the Supplemental Material [45], we show the effect of charge rescaling on both conductivity and transference number. While rescaling does lead to better agreement between experimental and theoretical conductivities (see Fig. S6 in Supplemental Material [45]), it has a negligible effect on the transference number. The decrease of t_+^0 to nearly zero at $r = 0.08$ reflects the increasingly dominant effect of solvent motion. From Eq. (2), we see that t_+^0 approaches zero when the cation and solvent velocities are similar. This occurs in the vicinity of $r_c = 0.08$, defined as the critical salt concentration.

Snapshots from MD simulations uncover the microscopic solvation shells that surround different Li^+ cations. Li^+ ions are solvated by oxygens either on the tetraglyme chains or from the $TFSI^-$ anions. At low concentrations, the average number of tetraglyme solvent molecules surrounding each Li^+ ion is two, while at high salt concentration, fewer solvent molecules coordinate to Li^+, implying that anions enter the solvation shells [Fig. 3(a)]. These two solvation motifs are depicted in Fig. 3(a), inset. The two-chain motif (left), comprising one cation and two solvent molecules, is predominant in the dilute regime ($r < 0.08$). In the concentrated regime ($r \geq 0.08$), the one-chain motif (right), comprising a cation coordinated by one solvent molecule and one anion, becomes increasingly important.

To understand solvent motion in the context of solvation structure, we quantify the fractions of the tetraglyme solvent within the two motifs [Fig. 3(b)]. The fraction of solvent in the two-chain motif increases until the critical salt concentration $r_c = 0.08$, and then decreases gradually. At $r > r_c$, the available solvent molecules are insufficient to fully solvate all lithium ions, resulting in an increase of the fraction of solvent molecules in the one-chain motif. In fact, the critical salt concentration $r_c = 0.08$ is remarkably close to a simplistic prediction based on two solvent molecules coordinating with each cation: $r = 1/(2 \times 5) = 0.1$ (each tetraglyme contains five O atoms). In Fig. 3(b), we also present the solvent velocity data measured by eNMR. The concentration dependence of v_0 parallels that of the fraction of solvent molecules in two-chain motifs; v_0 is also maximized at r_c. This result provides the molecular underpinning of $t_+^0 \approx 0$ at r_c: this is the concentration at which nearly all the solvent molecules lie within the solvation shells of Li^+. At higher concentrations, anions begin to replace solvent molecules in the solvation shells. One may view r_c as the salt concentration at which the dynamic heterogeneity of solvent motion is minimized.

Quantitative information about solvation structure from MD supports a simple model of solvent motion, in which we can calculate the solvation shell velocity, v_{shell}, under an

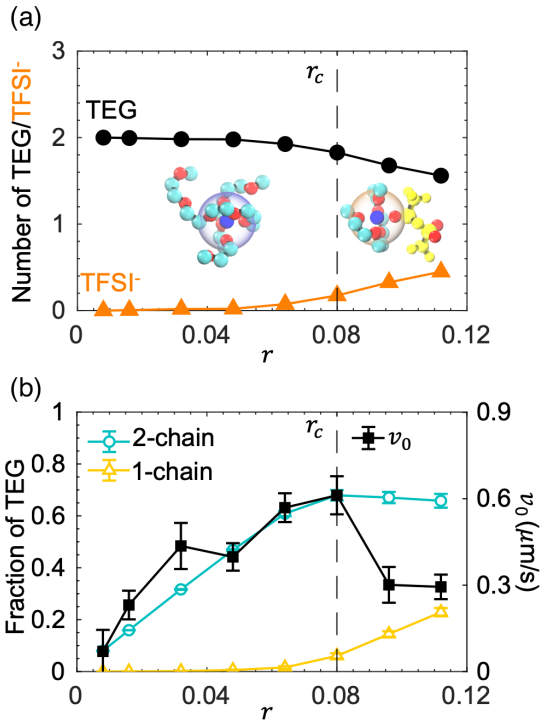

FIG. 3. (a) Average number of tetraglyme molecules (TEG, circles) and anions ($TFSI^-$, triangles) in the coordination shell of each Li^+ cation, obtained from MD. A tetraglyme molecule or $TFSI^-$ anion is determined to coordinate Li^+ if one of its oxygen atoms lies within 0.3 nm of Li^+. The insets, representative snapshots from simulations, depict the two-chain motif that dominates at low salt concentrations (left) and the one–chain motif that appears for $r > r_c$ (right); Li is shown in dark blue, C is shown in cyan and O in red; within $TFSI^-$, all atoms are shown in yellow except O in red. (b) Fraction of tetraglyme within the two-chain (open circles) and one-chain (open triangles) motifs, determined from MD. Solvent velocity measured by eNMR (filled squares) is overlaid using the right vertical axis, highlighting similar trends.

applied electric field. We posit that the solvent motion arises from the dragging of the solvent by the cation within a solvation shell. Our model accounts for the three dominant dynamically heterogeneous motifs that are evident in the simulations [Fig. 4(a)]: (i) the two-chain motif, (ii) the one-chain (with anion) motif, and (iii) free solvent molecules. The representative population of these motifs at $r = 0.08$ is shown in an MD snapshot of solvent molecules and Li^+ cations [Fig. 4(b)]. Since motifs (ii) and (iii) have no net charge, we assume that the measured solvent velocity simply reflects the fraction of solvent molecules in the two-chain motif (i). Thus solvent molecules within the two-chain motif [shown as blue chains in Fig. 4(b)] should translate with the cation under application of an electric field. The fractions quantified in Fig. 3 are thus directly related to the dynamic heterogeneity of solvent motion induced by the applied electric field. Breaking and reforming of the solvation structures occurs on a short timescale relative to the

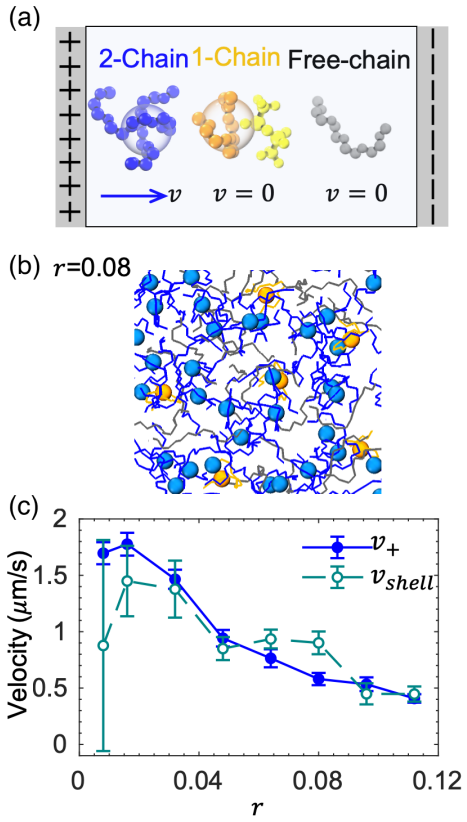

FIG. 4. Quantification of dynamic heterogeneity by estimating the drift velocity of only those solvent molecules that are in the solvation shell of the Li^+ cation. (a) Depiction of solvation motifs and free chains. In our model, only solvent molecules in the two-chain motif are dragged with the migrating cation (rightward arrow). The depicted electrodes are schematic. (b) MD snapshot of representative tetraglyme molecules (colored chains) and cations (spheres) at $r_c = 0.08$. The solvation motifs are highlighted using the same color scheme in (a). (c) Comparison of calculated shell velocity v_{shell} using Eq. (7) with measured cation velocity v_+ from eNMR. Error bars for v_{shell} reflect propagation of error in v_0 and f_2; both parameters approach zero as r tends to zero, resulting in large error bars. Velocities assume an applied electric field of 1 V/mm.

eNMR measurement (50 ms), and thus an individual solvent molecule will encounter all possible motifs such that its migration reflects an average over the populations dictated by dynamic speciation.

This simplified model relates the solvation shell velocity (v_{shell}) to the average solvent velocity by eNMR (v_0) and the fraction of solvent in the two-chain motif (f_2) from MD:

$$v_{\text{shell}} = \frac{v_0}{f_2}. \tag{7}$$

We can test the hypothesis that solvent motion under electric fields is due to two-chain motifs that are dragged by the migrating cation by comparing v_{shell} with v_+. This comparison, depicted in Fig. 4(c), shows the relationship between two independently measured quantities, v_0 and v_+. Agreement between v_{shell} and v_+ is observed within error across the range of salt concentrations. This validates our simple model and indicates that we can selectively quantify field-induced transport of only those solvent molecules within charged solvation shells in dynamically heterogeneous electrolytes.

At concentrations higher than those studied herein, multiple one-chain solvation motifs may share anions, thereby forming charged clusters [70–72] that will migrate and contribute to the solvent velocity. In prior computational work, negatively charged cation-anion clusters have been invoked to justify transference numbers in the vicinity of zero [27]. Our analysis suggests that $t_+^0 \approx 0$ may also arise entirely from cation-solvent correlations. Developing an experimentally validated framework that accounts for both ion-solvent and charged cation-anion clusters is an avenue for future work.

In summary, we present a novel approach for molecular interpretation of eNMR results using MD simulations in concentrated electrolytes. Our work establishes the importance of directly quantifying solvent motion, which has traditionally been a neglected variable in electrochemistry. The MD simulations reveal two dominant solvation motifs (i) where the cation is solvated by two solvent molecules, and (ii) where it is solvated by one solvent molecule and an anion. We validate a model of cation-solvent coordination that quantifies the velocity of only those solvent molecules that lie within solvation shells of the migrating Li^+ cations. The LiTFSI-tetraglyme electrolyte is dynamically heterogeneous at all salt concentrations; the cation transference number t_+^0 approaches zero in the least dynamically heterogeneous electrolyte.

This work was intellectually led by the Joint Center for Energy Storage Research (JCESR), an Energy Innovation Hub funded by the U.S. Department of Energy (DOE), Office of Science, Basic Energy Sciences (BES). We thank Dr. Jeffrey G. Pelton (California Institute for Quantitative Biosciences, UC Berkeley) for providing support that enabled the NMR measurements in this work, and Dr. Pavel V. Yushmanov (P&L Scientific, Sweden) for useful technical discussions regarding eNMR measurements. Lorena S. Grundy and Kranthi Mandadapadu (UC Berkeley) are gratefully acknowledged for helpful suggestions and discussions. Computational hours were provided by the Savio cluster at UC Berkeley and the Lawrencium cluster at LBNL.

*These authors contributed equally to this work.
†Corresponding author.
ruiwang325@berkeley.edu

[1] R. A. Robinson and R. H. Stokes, *Electrolyte Solutions* (Courier Corporation, New York, 2002).
[2] J. Newman and N. P. Balsara, *Electrochemical Systems* (John Wiley & Sons, New York, 2021).

[3] J. W. Hittorf, On the migration of ions during electrolysis, in *The Fundamental Laws of Electrolytic Conduction: Memoirs by Faraday, Hittorf, and F. Kohlrausch* (Harper & Brothers, New York, 1899).

[4] W. Hittorf, Das Verhalten der Diaphragmen bei der Elektrolyse von Salzlösungen, Z. Phys. Chem. **43U**, 239 (1903).

[5] L. Onsager, Reciprocal relations in irreversible processes. I., Phys. Rev. **37**, 405 (1931).

[6] L. Onsager, Reciprocal relations in irreversible processes. II., Phys. Rev. **38**, 2265 (1931).

[7] J. Newman, D. Bennion, and C. W. Tobias, Mass transfer in concentrated binary electrolytes, Ber. Bunsenges. Phys. Chem. **69**, 608 (1965).

[8] M. D. Ediger, Spatially heterogeneous dynamics in supercooled liquids, Annu. Rev. Phys. Chem. **51**, 99 (2000).

[9] C. A. Angell, K. L. Ngai, G. B. McKenna, P. F. McMillan, and S. W. Martin, Relaxation in glassforming liquids and amorphous solids, J. Appl. Phys. **88**, 3113 (2000).

[10] Y.-L. Wang, B. Li, S. Sarman, F. Mocci, Z.-Y. Lu, J. Yuan, A. Laaksonen, and M. D. Fayer, Microstructural and dynamical heterogeneities in ionic liquids, Chem. Rev. **120**, 5798 (2020).

[11] B. J. Morgan, Understanding fast-ion conduction in solid electrolytes, Phil. Trans. R. Soc. A **379**, 20190451 (2021).

[12] Y. Ma, M. Doyle, T. F. Fuller, M. M. Doeff, L. C. D. Jonghe, and J. Newman, The measurement of a complete set of transport properties for a concentrated solid polymer electrolyte solution, J. Electrochem. Soc. **142**, 1859 (1995).

[13] K. M. Diederichsen, E. J. McShane, and B. D. McCloskey, Promising routes to a high Li^+ transference number electrolyte for lithium ion batteries, ACS Energy Lett. **2**, 2563 (2017).

[14] R. L. Snyder, Y. Choo, K. W. Gao, D. M. Halat, B. A. Abel, S. Sundararaman, D. Prendergast, J. A. Reimer, N. P. Balsara, and G. W. Coates, Improved Li^+ transport in polyacetal electrolytes: Conductivity and current fraction in a series of polymers, ACS Energy Lett. **6**, 1886 (2021).

[15] P. Barai, K. Higa, and V. Srinivasan, Lithium dendrite growth mechanisms in polymer electrolytes and prevention strategies, Phys. Chem. Chem. Phys. **19**, 20493 (2017).

[16] L. Frenck, G. K. Sethi, J. A. Maslyn, and N. P. Balsara, Factors that control the formation of dendrites and other morphologies on lithium metal anodes, Front. Energy Res. **7**, 115 (2019).

[17] J. Newman, Transport processes in electrolytic solutions, in *Advances in Electrochemistry and Electrochemical Engineering* (Interscience Publishers New York, 1967), Vol. 5, pp. 87–136.

[18] M. Holz, Electrophoretic NMR, Chem. Soc. Rev. **23**, 165 (1994).

[19] H. J. Walls and T. A. Zawodzinski, Anion and cation transference numbers determined by electrophoretic NMR of polymer electrolytes sum to unity, Electrochem. Solid-State Lett. **3**, 321 (2000).

[20] F. Hallberg, I. Furó, P. V. Yushmanov, and P. Stilbs, Sensitive and robust electrophoretic NMR: Instrumentation and experiments, J. Magn. Reson. **192**, 69 (2008).

[21] M. Gouverneur, J. Kopp, L. van Wüllen, and M. Schönhoff, Direct determination of ionic transference numbers in ionic liquids by electrophoretic NMR, Phys. Chem. Chem. Phys. **17**, 30680 (2015).

[22] K. Timachova, J. Newman, and N. P. Balsara, Theoretical interpretation of ion velocities in concentrated electrolytes measured by electrophoretic NMR, J. Electrochem. Soc. **166**, A264 (2019).

[23] L. S. Grundy, D. B. Shah, H. Q. Nguyen, K. M. Diederichsen, H. Celik, J. M. DeSimone, B. D. McCloskey, and N. P. Balsara, Impact of frictional interactions on conductivity, diffusion, and transference number in ether- and perfluoroether-based electrolytes, J. Electrochem. Soc. **167**, 120540 (2020).

[24] O. Borodin and G. D. Smith, Mechanism of ion transport in amorphous poly(ethylene oxide)/LiTFSI from molecular dynamics simulations, Macromolecules **39**, 1620 (2006).

[25] D. R. Wheeler and J. Newman, Molecular dynamics simulations of multicomponent diffusion. 1. Equilibrium method, J. Phys. Chem. B **108**, 18353 (2004).

[26] D. R. Wheeler and J. Newman, Molecular dynamics simulations of multicomponent diffusion. 2. Nonequilibrium method, J. Phys. Chem. B **108**, 18362 (2004).

[27] A. France-Lanord and J. C. Grossman, Correlations from Ion Pairing and the Nernst-Einstein Equation, Phys. Rev. Lett. **122**, 136001 (2019).

[28] N. M. Vargas-Barbosa and B. Roling, Dynamic ion correlations in solid and liquid electrolytes: How do they affect charge and mass transport?, Chem. Electro. Chem. **7**, 367 (2020).

[29] K. D. Fong, H. K. Bergstrom, B. D. McCloskey, and K. K. Mandadapu, Transport phenomena in electrolyte solutions: Nonequilibrium thermodynamics and statistical mechanics, AIChE J. **66**, e17091 (2020).

[30] R. Hayes, G. G. Warr, and R. Atkin, Structure and nanostructure in ionic liquids, Chem. Rev. **115**, 6357 (2015).

[31] T. Méndez-Morales, J. Carrete, Ó. Cabeza, O. Russina, A. Triolo, L. J. Gallego, and L. M. Varela, Solvation of lithium salts in protic ionic liquids: A molecular dynamics study, J. Phys. Chem. B **118**, 761 (2014).

[32] L. M. Varela, T. Méndez-Morales, J. Carrete, V. Gómez-González, B. Docampo-Álvarez, L. J. Gallego, O. Cabeza, and O. Russina, Solvation of molecular cosolvents and inorganic salts in ionic liquids: A review of molecular dynamics simulations, J. Mol. Liq. **210**, 178 (2015).

[33] K. Shimizu, A. A. Freitas, R. Atkin, G. G. Warr, P. A. FitzGerald, H. Doi, S. Saito, K. Ueno, Y. Umebayashi, M. Watanabe, and J. N. C. Lopes, Structural and aggregate analyses of (Li salt + glyme) mixtures: The complex nature of solvate ionic liquids, Phys. Chem. Chem. Phys. **17**, 22321 (2015).

[34] W. A. Henderson, D. M. Seo, S.-D. Han, and O. Borodin, Electrolyte solvation and ionic association. VII. Correlating Raman spectroscopic data with solvate species, J. Electrochem. Soc. **167**, 110551 (2020).

[35] I. Prigogine, *Introduction to Thermodynamics of Irreversible Processes* (Interscience, New York, 1967).

[36] S. R. De Groot and P. Mazur, *Non-equilibrium Thermodynamics* (Courier Corporation, New York, 2013).

[37] K. D. Fong, J. Self, B. D. McCloskey, and K. A. Persson, Onsager transport coefficients and transference numbers in polyelectrolyte solutions and polymerized ionic liquids, Macromolecules **53**, 9503 (2020).

[38] K. D. Fong, J. Self, B. D. McCloskey, and K. A. Persson, Ion correlations and their impact on transport in polymer-based electrolytes, Macromolecules **54**, 2575 (2021).
[39] D. T. Hallinan and N. P. Balsara, Polymer electrolytes, Annu. Rev. Mater. Res. **43**, 503 (2013).
[40] K. Timachova, H. Watanabe, and N. P. Balsara, Effect of molecular weight and salt concentration on ion transport and the transference number in polymer electrolytes, Macromolecules **48**, 7882 (2015).
[41] D. M. Halat, R. L. Snyder, S. Sundararaman, Y. Choo, K. W. Gao, Z. J. Hoffman, B. A. Abel, L. S. Grundy, M. D. Galluzzo, M. P. Gordon, H. Celik, J. J. Urban, D. Prendergast, G. W. Coates, N. P. Balsara, and J. A. Reimer, Modifying Li^+ and anion diffusivities in polyacetal electrolytes: A pulsed-field-gradient NMR study of ion self-diffusion, Chem. Mater. **33**, 4915 (2021).
[42] Y. Fang, P. V. Yushmanov, and I. Furó, Improved accuracy and precision in electrophoretic NMR experiments. Current control and sample cell design, J. Magn. Reson. **318**, 106796 (2020).
[43] Q. He and Z. Wei, Convection compensated electrophoretic NMR, J. Magn. Reson. **150**, 126 (2001).
[44] Z. Zhang and L. A. Madsen, Observation of separate cation and anion electrophoretic mobilities in pure ionic liquids, J. Chem. Phys. **140**, 084204 (2014).
[45] See Supplemental Material at http://link.aps.org/supplemental/10.1103/PhysRevLett.128.198002 for electrolyte preparation, conductivity probe measurements, eNMR measurements, MD simulations, and Onsager transport coefficients.
[46] C. Ammann, P. Meier, and A. Merbach, A simple multinuclear NMR thermometer, J. Magn. Reson. **46**, 319 (1982).
[47] W. M. Spees, S.-K. Song, J. R. Garbow, J. J. Neil, and J. J. H. Ackerman, Use of ethylene glycol to evaluate gradient performance in gradient-intensive diffusion MR sequences, Magn. Reson. Med. **68**, 319 (2012).
[48] R. M. Cotts, M. J. R. Hoch, T. Sun, and J. T. Markert, Pulsed field gradient stimulated echo methods for improved NMR diffusion measurements in heterogeneous systems, J. Magn. Reson. **83**, 252 (1989).
[49] Y. Fang, P. V. Yushmanov, and I. Furó, Improved accuracy and precision in electrophoretic NMR experiments. Current control and sample cell design, J. Magn. Reson. **318**, 106796 (2020).
[50] R. L. Kay and D. F. Evans, The conductance of the tetraalkylammonium halides in deuterium oxide solutions at 25°, J. Phys. Chem. **69**, 4216 (1965).
[51] A. Jerschow and N. Müller, Convection compensation in gradient enhanced nuclear magnetic resonance spectroscopy, J. Magn. Reson. **132**, 13 (1998).
[52] E. Pettersson, I. Furó, and P. Stilbs, On experimental aspects of electrophoretic NMR, Concepts Magn. Reson., Part A **22A**, 61 (2004).
[53] K. Shigenobu, K. Dokko, M. Watanabe, and K. Ueno, Solvent effects on Li ion transference number and dynamic ion correlations in glyme- and sulfolane-based molten Li salt solvates, Phys. Chem. Chem. Phys. **22**, 15214 (2020).
[54] K. Shigenobu, M. Shibata, K. Dokko, M. Watanabe, K. Fujii, and K. Ueno, Anion effects on Li ion transference number and dynamic ion correlations in glyme–Li salt equimolar mixtures, Phys. Chem. Chem. Phys. **23**, 2622 (2021).
[55] F. Schmidt and M. Schönhoff, Solvate cation migration and ion correlations in solvate ionic liquids, J. Phys. Chem. B **124**, 1245 (2020).
[56] H. Gudla, C. Zhang, and D. Brandell, Effects of solvent polarity on Li-ion diffusion in polymer electrolytes: An all-atom molecular dynamics study with charge scaling, J. Phys. Chem. B **124**, 8124 (2020).
[57] M. J. Abraham, T. Murtola, R. Schulz, S. Páll, J. C. Smith, B. Hess, and E. Lindahl, GROMACS: High performance molecular simulations through multi-level parallelism from laptops to supercomputers, SoftwareX **1–2**, 19 (2015).
[58] B. Hess, H. Bekker, H. J. C. Berendsen, and J. G. E. M. Fraaije, LINCS: A linear constraint solver for molecular simulations, J. Comput. Chem. **18**, 1463 (1997).
[59] G. Bussi, D. Donadio, and M. Parrinello, Canonical sampling through velocity rescaling, J. Chem. Phys. **126**, 014101 (2007).
[60] H. J. C. Berendsen, J. P. M. Postma, W. F. van Gunsteren, A. DiNola, and J. R. Haak, Molecular dynamics with coupling to an external bath, J. Chem. Phys. **81**, 3684 (1984).
[61] T. Darden, D. York, and L. Pedersen, Particle mesh Ewald: An N·log(N) method for Ewald sums in large systems, J. Chem. Phys. **98**, 10089 (1993).
[62] H. Wu and C. D. Wick, Computational investigation on the role of plasticizers on ion conductivity in poly(ethylene oxide) LiTFSI electrolytes, Macromolecules **43**, 3502 (2010).
[63] B. M. Savoie, M. A. Webb, and T. F. Miller, Enhancing cation diffusion and suppressing anion diffusion via Lewis-acidic polymer electrolytes, J. Phys. Chem. Lett. **8**, 641 (2017).
[64] S. Tsuzuki, W. Shinoda, M. Matsugami, Y. Umebayashi, K. Ueno, T. Mandai, S. Seki, K. Dokko, and M. Watanabe, Structures of $[Li(glyme)]^+$ complexes and their interactions with anions in equimolar mixtures of glymes and Li[TFSA]: Analysis by molecular dynamics simulations, Phys. Chem. Chem. Phys. **17**, 126 (2015).
[65] A. Thum, A. Heuer, K. Shimizu, and J. N. Canongia Lopes, solvate ionic liquids based on lithium bis(trifluoromethanesulfonyl)imide–glyme systems: Coordination in MD simulations with scaled charges, Phys. Chem. Chem. Phys. **22**, 525 (2020).
[66] C. D. Wick and D. N. Theodorou, Connectivity-altering Monte Carlo simulations of the end group effects on volumetric properties for poly(ethylene oxide), Macromolecules **37**, 7026 (2004).
[67] J. N. Canongia Lopes and A. A. H. Pádua, Molecular force field for ionic liquids composed of triflate or bistriflylimide anions, J. Phys. Chem. B **108**, 16893 (2004).
[68] C. Do, P. Lunkenheimer, D. Diddens, M. Götz, M. Weiß, A. Loidl, X.-G. Sun, J. Allgaier, and M. Ohl, Li^+ Transport in Poly(Ethylene Oxide) Based Electrolytes: Neutron Scattering, Dielectric Spectroscopy, and Molecular Dynamics Simulations, Phys. Rev. Lett. **111**, 018301 (2013).
[69] D. J. Brooks, B. V. Merinov, W. A. Goddard, B. Kozinsky, and J. Mailoa, Atomistic description of ionic diffusion in PEO–LiTFSI: Effect of temperature, molecular weight,

and ionic concentration, Macromolecules **51**, 8987 (2018).
[70] T. Murphy, S. K. Callear, N. Yepuri, K. Shimizu, M. Watanabe, J. N. Canongia Lopes, T. Darwish, G. G. Warr, and R. Atkin, Bulk nanostructure of the prototypical 'good' and 'poor' solvate ionic liquids [Li(G4)][TFSI] and [Li(G4)][NO_3], Phys. Chem. Chem. Phys. **18**, 17224 (2016).
[71] A. Kitada, K. Kawata, M. Shimizu, M. Saimura, T. Nagata, M. Katahira, K. Fukami, and K. Murase, Ligand exchange conduction of lithium ion in a pentaglyme-lithium bis (trifluoromethylsulfonyl)amide super-concentrated electrolyte, J. Electrochem. Soc. **168**, 016506 (2021).
[72] A. Kitada, Y. Koujin, M. Shimizu, K. Kawata, C. Yoshinaka, M. Saimura, T. Nagata, M. Katahira, K. Fukami, and K. Murase, Glyme-lithium bis(trifluoromethylsulfonyl)amide super-concentrated electrolytes: Salt addition to solvate ionic liquids lowers ionicity but liberates lithium ions, J. Electrochem. Soc. **168**, 090521 (2021).